



Quantum aggregation with temporal delay

Nicolò Lo Piparo ^{1,*}, William J. Munro ^{1,2} and Kae Nemoto^{1,2}

¹*Okinawa Institute of Science and Technology Graduate University, 1919-1 Tancha, Onna-son, Okinawa 904-0495, Japan*

²*National Institute of Informatics, 2-1-2 Hitotsubashi, Chiyoda-ku, Tokyo 101-8430, Japan*



(Received 4 April 2024; accepted 6 September 2024; published 13 September 2024)

Advanced quantum networking systems rely on efficient quantum error correction codes for their optimal realization. The rate at which the encoded information is transmitted is a fundamental limit that affects the performance of such systems. Quantum aggregation allows one to increase the transmission rate by adding multiple paths connecting two distant users. Aggregating channels of different paths allows more users to simultaneously exchange the encoded information. Recent work has shown that quantum aggregation can also reduce the number of physical resources of an error correction code when it is combined with the quantum multiplexing technique. However, the difference in channel lengths across the various paths means some of the encoded quantum information will arrive earlier than others and it must be stored in quantum memories. The information stored will then deteriorate due to decoherence processes leading to detrimental effects for the fidelity of the final quantum state. Here, we explore the effects of a depolarization channel that occurs for the quantum Reed-Solomon code when quantum aggregation involving different channel lengths is used. We determine the best distribution of resources among the various channels connecting two remote users. Furthermore, we estimate the coherence time required to achieve a certain fidelity. Our results will have a significant impact on the ways physical resources are distributed across a quantum network.

DOI: [10.1103/PhysRevA.110.032613](https://doi.org/10.1103/PhysRevA.110.032613)

I. INTRODUCTION

Future quantum networks will allow one to exchange information over large distances connecting multiple remote users [1–3]. This can be accomplished by sending high-quality quantum states, which can then be used for a variety of tasks, for instance, improving the security of the communication channels using quantum cryptographic protocols [4–10], accelerating the computational time with quantum computers [11–16], and improving the precision of measurements with quantum sensing and imaging methods [17–19]. However, due to the fragile nature of these quantum states errors and device imperfections will affect the performance of those approaches canceling the advantages that these technologies have on their classical counterparts.

One method that allows the transmission of high-fidelity states involves the use of quantum error correction (QEC) codes [20–26]. Information is now encoded in a more complex quantum system, which protects it from the errors occurring during transmission and recovered when needed. The complexity of such a code requires a large number of physical resources for the encoding. Communication channels with low capacities [27–29] and insufficient resources within a node will reduce the number of resources that can be transmitted over a single path, greatly affecting the communication rate. For instance, when several users are connected by the same path (or part of it), the number of channels of the path can be insufficient for an efficient communication between two users, decreasing thus their communication rate. Alternatively, one can think of a single channel connecting two users.

The communication rate, in this case, will be strictly limited by the repetition rate at which the photons are sent.

One way to alleviate these issues is to connect the users with more paths using quantum aggregation in which the encoded states are distributed over the channels of those distinct paths [30]. This allows a user at the sender's node to immediately communicate with the users at the receiver node without the necessity of waiting for the connecting channels to be available after the other users end their communication tasks. In Ref. [30] it was shown that using two paths for exchanging information using the quantum Reed-Solomon [31] (QRS) code allows one to use channels of higher quality to compensate for other channels of lower quality and still reach the threshold fidelity. For instance, to reach a threshold fidelity of the encoded transmitted state equal to 99.5% a user can send his state over two paths, one having channel loss transmission probability 20% higher and the other one having channel loss transmission probability 50% lower compared to the channel loss transmission probability of the single-path case [30]. Moreover, when higher-dimensional photonic encodings are used [32] quantum aggregation shows a drastic reduction of the physical resources required to reach a threshold fidelity [30].

In the aggregation scenario, a fundamental issue arises due to the different length of the two paths. In fact, part of the encoded information that arrives early at the remote node must be stored in quantum memories, which undergoes a dephasing process affecting the final fidelity of the state [33]. Once the delayed piece of encoded state reaches the far end, it can be used with the one retrieved from the quantum memory to correct the errors. The coherence time of the quantum memories used can, therefore, play a fundamental role in determining

*Contact author: nicopale@gmail.com

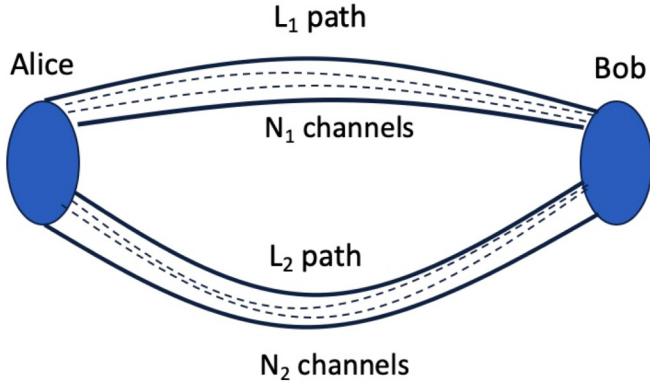


FIG. 1. Quantum aggregation over two paths of length $L_2 > L_1$ containing each N_1 , N_2 channels, respectively. Alice distributes her encoded state over the channels and sends it through the two paths. Bob stores the received early qudits into quantum memories and decodes the state once the delayed qudits have arrived.

the performance of the QEC code when quantum aggregation is in use. Large path-length differences or short coincidence times can be detrimental in recovering the information sent making the communication among users impossible. A low coherence time might also determine whether adopting quantum aggregation is a valid option to reach a certain threshold fidelity.

In this work we analyze the impact of temporal delays caused by the path-length differences (i.e., the time interval in which a piece of an encoded quantum state is stored and that one in which it is retrieved) on the fidelity of the final decoded state in a quantum aggregation scenario. To this end, we consider two users that exchange information using the QRS code connected by two and three communication paths of different lengths. We determine the performance of such a system with delay for several configurations in which the information can be distributed and we determine the coherence times the quantum memories must have for an optimal performance. The paper is divided as follows. In Sec. II we analyze a quantum aggregation system applied to the smallest QRS code with a temporal delay in one path. Then in Sec. III we extend our analysis to higher-dimensional QRS codes and show several different and interesting configuration arise. We conclude in Sec. IV.

II. QUANTUM AGGREGATION WITH DELAY

Let us begin by exploring the effect of temporal delay in quantum aggregation using the $[[n, 1, d]]_D$ QRS code, where n is the number of physical qudits of dimension D used to encode one logical qudit and capable of correcting the loss of $d - 1$ qudits, with d being the code distance. In the general quantum aggregation scenario two users, Alice and Bob, are connected by two lossy paths having different lengths L_1 and L_2 , as shown in Fig. 1. In the following we assume that $D = n = N_1 + N_2$ with N_1 and N_2 being the number of channels inside path 1 and path 2, respectively, and $L_2 > L_1$ [33]. Alice encodes her state using a $[[n, 1, d]]_D$ QRS code and distributes N_1 qudits in the channels of path 1 and N_2 qudits in the channels of path 2, respectively. We denote such

a configuration as $N_1 + N_2$. Then Bob decodes the received states if the number of the transmitted qudits arriving earlier (N'_1) is enough for retrieving the information sent by Alice ($N'_1 \geq d$), otherwise, when $N'_1 < d$, he stores those qudits in quantum memories (QMs). We assume that the density matrix, ρ , of these stored qudits that undergo a depolarizing channel is given by $\rho \rightarrow \rho' = (1 - p_d)\rho + p_d I/D'$, where I is the D' -dimensional identity operator and p_d is the depolarization error probability given by $p_d = 1 - e^{-t/T_2}$, with $t = (L_2 - L_1)/c$, with c being the speed of light traveling in optical fibers and T_2 being the coherence time of the QMs. Next when $N'_1 < d$ while the number of qudits transmitted over path 2 (N'_2) satisfies $N'_2 \geq d$, Bob uses the N'_2 qudits to recover the initial information discarding the stored qudits associated with the transmission through path L_1 . Now when both $N'_1 < d$ and $N'_2 < d$ but with $N'_1 + N'_2 \geq d$ Bob retrieves the qudits stored into the QMs and applies a decoding procedure on all transmitted qudits. This later case will affect the fidelity of the decoded state due to the *temporal delay* of the qudits traveling in path 2. Finally, when $N'_1 + N'_2 < d$ we assume for simplicity the state shared by Alice and Bob is a completely mixed state (the worst case) and all the information has been lost. We assume that the local gates' errors are negligible compared to the memory depolarization errors.

Now let us explore the impact of the temporal delay in a quantum aggregation scenario using the smallest QRS code the $[[3, 1, 2]]_3$ code capable of correcting one error in which one logic qutrit is created using three physical qutrits. In the $[[3, 1, 2]]_3$ QRS code protocol Alice encodes her initial qutrit $|\psi\rangle_A = \alpha_0|0\rangle + \alpha_1|1\rangle + \alpha_2|2\rangle$ into the logic state $|\psi\rangle_L = \alpha_0|0\rangle_L + \alpha_1|1\rangle_L + \alpha_2|2\rangle_L$, where $|0\rangle_L = (|000\rangle + |111\rangle + |222\rangle)/\sqrt{3}$; $|1\rangle_L = (|012\rangle + |120\rangle + |201\rangle)/\sqrt{3}$ and $|2\rangle_L = (|021\rangle + |102\rangle + |210\rangle)/\sqrt{3}$. She sends this encoded state over a lossy path to Bob. Upon a successful transmission of the state sent by Alice, Bob applies a decoding procedure described in Muralidharam *et al.* [34] to retrieve the initial state. In the quantum aggregation scenario, we have two configurations; the 2 + 1 configuration and the 1 + 2 configuration, in which 2(1) qudits are traveling in the channels of path 1 having a transmissivity $p_1 = e^{-L_1/L_{\text{att}}}$ while 1(2) qutrits are sent via path 2 with transmission probability $p_2 = e^{-L_2/L_{\text{att}}}$, respectively. Here $L_{\text{att}} = 22$ km (0.2 dB/km) is the attenuation length of the optical fiber.

In the 2 + 1 configuration the fidelity F_{2+1} of the state received and decoded by Bob is

$$F_{2+1} = p_1^2 p_2 + 2p_1 p_2 (1 - p_1) \left(1 - \frac{2}{3} p_d\right) + p_1^2 (1 - p_2) + (1 - P_{s_1})/27, \quad (1)$$

where $P_{s_1} = p_1^2 p_2 + 2p_1 p_2 (1 - p_1) + p_1^2 (1 - p_2)$ is the probability of the successful transmission of information from Alice to Bob. Let us give an intuitive derivation of Eq. (1) that can be easily extended to derive the fidelity of higher-dimensional QRS codes. The no-loss term, which is the first and dominant term in Eq. (1), and the loss of the qudit traveling in path 2 [third term in Eq. (1)] do not depend on the depolarization error p_d because Bob immediately applies the decoding procedure on the two qutrits traveling in the channels of path 1. Then, in the case in which one of the two qudits traveling in path 1 is lost, the temporal delay due to

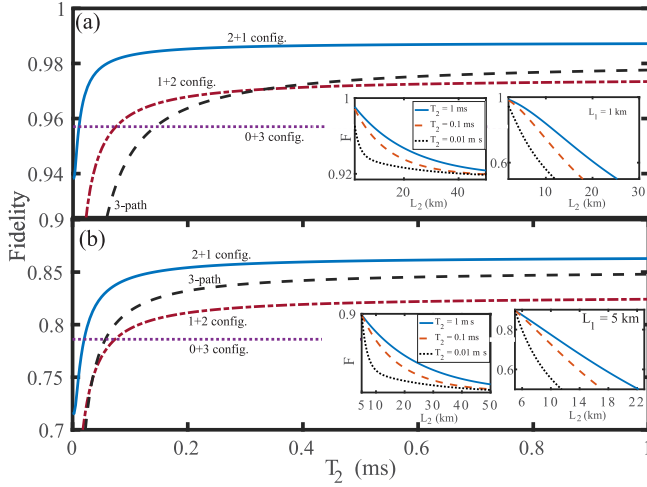


FIG. 2. Fidelity of the decoded state received by Bob versus the coherence time, T_2 , of the QM used to store the qutrits transmitted through path 1, in the 2 + 1 configuration (solid blue lines) and 1 + 2 configuration (dash-dotted red lines) for (a) $L_1 = 1$ km, $L_2 = 3$ km and (b) $L_1 = 5$ km, $L_2 = 8$ km. In the insets we depict the fidelity, F , versus L_2 at (a) $L_1 = 1$ km and (b) $L_1 = 5$ km for both configurations. Also shown for the three-path configuration as the black dashed curves (a) with $L_1 = 1$ km, $L_2 = 2$ km, $L_3 = 3$ km and (b) with $L_1 = 5$ km, $L_2 = 6$ km, $L_3 = 8$ km. The dotted purple lines are the fidelities of the 0 + 3 configuration (where the length of the channels in path 1 are increased so $L_1 = L_2$).

the storage of the transmitted qutrit contributes to the fidelity with a term proportional to $(1 - \frac{2}{3}p_d)$, which is derived in Appendix A. To gain an understanding of the behavior of the fidelity we plot in Fig. 2(a) the fidelity F_{2+1} versus the memories coherence time for $L_1 = 1$ km and $L_2 = 3$ km (solid blue curve). We see that the coherence time of the QM only affects the fidelity when $T_2 < 0.1$ ms and noting that for no memory ($T_2 = 0$) $F_{2+1} \sim 0.94$. This is due to the fact that the no-loss term does not depend on p_d . Therefore, even when there are no QMs in the system the transmitted state can be used to extract some information. A similar explanation can be given to the case in which $L_2 \rightarrow \infty$ [see the left graph of the inset of Fig. 2(a)]. Here we plot the fidelity versus L_2 with $L_1 = 1$ km for $T_2 = 1$ ms (solid blue curve), $T_2 = 0.1$ ms (dashed red curve), and $T_2 = 0.01$ ms, respectively. We observe that the fidelity decreases at lower coherence times while reaching an asymptotic value of ~ 0.92 at large values of L_2 , from which information can partially be extracted. This can be explained considering that, for this configuration, the no-loss term corresponds to the case in which two qutrits are successfully transmitted and one is lost with very high probability. Therefore, since this code can correct the loss of one qutrit, the transmitted state containing two qutrits with probability ($\sim p_1^2$) still has sufficient information allowing the fidelity to exceed 50%.

The alternate 1 + 2 configuration changes quite drastically. It is straightforward to show that F_{1+2} is

$$F_{1+2} = p_2^2 p_1 + 2p_1 p_2 (1 - p_2) \left(1 - \frac{2}{3} p_d\right) + p_2^2 (1 - p_1) + (1 - P_{s_2})/27, \quad (2)$$

where $P_{s_2} = p_2^2 p_1 + 2p_1 p_2 (1 - p_2) + p_2^2 (1 - p_1)$. Even in this configuration the dominant term is the no-loss term, which does not depend on p_d because, although the two qutrits arrive later, they can be immediately used to decode the state while discarding the early qutrit transmitted over path 1. The second term in Eq. (2) refers to the loss of a qutrit traveling in path 2. Therefore, Bob needs to retrieve the stored qutrit from the QM to decode the state together with the single qutrit transmitted over path 2. The contribution to the fidelity from the depolarization channel applied to the stored qutrit is equal to the previous configuration. Finally, the third term in Eq. (2) does not depend on p_d because Bob can use the two qutrits transmitted over path 2 to decode the state. To visualize this we plot F_{2+1} (solid red line) versus T_2 at the same numerical values of the previous configuration, as shown in Fig. 2(a). As expected, the fidelity in this case has much lower values because the no-loss term suffers the loss of two qutrits with higher probability, hence the second term in Eq. (2) is more relevant in this case. In other words, the coherence time in this case affects the fidelity more than the other case. This can also be seen from the graph in the right side of the inset of Fig. 2(a). Here, we plot the fidelity versus L_2 for different coherence times. In this case the probability of losing two qutrits traveling in path 2 increases with L_2 , [mathematically, the first term in Eq. (2) decreases], hence, the contribution to the fidelity from the second term is more significant. In this case one can see that T_2 determines a threshold value for L_2 after which the fidelity is below 50% [see the crossing points of the curves with the x axis in the graph in the right side of the inset of Fig. 2(a)]. From this considerations we conclude (as expected) that distributing more qutrits in the shorter channel gives a significant advantage in terms of having higher fidelities and being slightly affected by the coherence time. Please see Appendix B for the full derivation of Eqs. (1) and (2).

We expect that, for higher values of L_1 , all the results described above are worse for both configurations. This scenario is shown in Fig. 2(b), where we plot the fidelities of the configurations versus T_2 at $L_1 = 5$ km and $L_2 = 8$ km and in the inset where we plot the fidelities of both configurations versus L_2 at $L_1 = 5$ km. Even in this case the fidelity in the 2 + 1 configuration reaches an asymptotic value as L_2 increases, which is much lower than the previous case.

It is interesting now to add one more path (path 3), with transmission probability $p_3 = e^{-L_3/L_{att}}$, to the previous scheme, such that $L_3 > L_2 > L_1$ while maintaining the same highest distance separating Alice and Bob. In this case, each qutrit travels across a channel in the corresponding path. This can be referred to as the 1 + 1 + 1 configuration. The fidelity of Bob's decoded state is

$$F_{1+1+1} = p_1 p_2 p_3 \left(1 - \frac{2}{3} p_{d_{12}}\right) + (1 - P_s) 1/27 + \sum_{i \neq j \neq k=1}^3 p_i p_j (1 - p_k) \left(1 - \frac{2}{3} p_{d_{ij}}\right), \quad (3)$$

where $p_{d_{ij}} = 1 - e^{-T_{ij}/T_2}$, with $T_{ij} = |L_i - L_j|/c$ and $P_s = p_1 p_2 p_3 + p_2 p_3 (1 - p_1) + p_1 p_3 (1 - p_2) + p_1 p_2 (1 - p_3)$. In this case, the no-loss term of Eq. (3) depends on p_d because the qutrit traveling in the channel of path 1 arrives first and

needs to be stored in a QM before Bob can apply a decoding process with a second qudit. One can also see that all the other terms in Eq. (3) depends on p_d because, in the loss event of any qudit, Bob needs to wait for another one to start the decoding process. Figure 2(a) shows the fidelity of Eq. (3) (black dashed line) at $L_1 = 1$ km, $L_2 = 2$ km, and $L_3 = 3$ km. One can see that, for small values of T_2 ($T_2 < 0.1$ ms), the no-loss term greatly affects the fidelity, whereas for higher values of T_2 the fidelity of the three-path case increases until it crosses the 1 + 2 configuration of the two-path case at a crossing point $T_2^c \simeq 0.3$ ms. This is due to the fact that the expression of the fidelity of the state received by Bob in the three-path case is more affected by the coherence time than the 1 + 2 case as one can see comparing Eq. (1) with Eq. (3). Therefore, we expect that, for large values of T_2 , the no-loss term of Eq. (3) becomes higher than the no-loss term of Eq. (1) because when $T_2 \rightarrow \infty$ the qudit in path 2 travels over a smaller distance than the qudits of the 1 + 2 configuration. At $L_1 = 5$ km and $L_2 = 8$ km the three-path case has also a lower fidelity as shown from the dashed curve in Fig. 2(b). However, in this case the crossing point of this curve with the one corresponding to the 1 + 2 configuration is slightly lower than the crossing point shows in Fig. 2(a). This can be explained by considering that, for larger distances, the main source of error is the channel loss, hence, the coherence time affects less the fidelity of the decoded state. In fact, we can see that at very low values of T_2 the fidelity of the three-path case is very similar to the 1 + 2 case.

For comparison we also plot the fidelities of the 0 + 3 configuration (dotted purple line), as shown in Figs. 2(a) and 2(b). This corresponds to the situation in which the channel length of the shorter path has been increased so $L_1 = L_2$. One notices that the 0 + 3 case outperforms both the 2 + 1 and 1 + 2 case as well as the three-path case at low values of T_2 . This shows that for a very limited range of low decoherence times it might be more convenient adding a fiber delay line to the shorter path to match the longer path rather than using quantum aggregation.

III. TEMPORAL DELAY FOR HIGHER-DIMENSIONAL CODES

So far we considered the smallest QRS code that can correct one loss errors. What happens as we increase the code size? We analyze the effects of the temporal delay in a quantum aggregation scenario for the $[[5, 1, 3]]_5$ and the $[[7, 1, 4]]_7$, QRS codes, which can fix the loss of two and three qudits, respectively. Let us begin with the $[[5, 1, 3]]_5$ code. Here there are four possible configurations: 4 + 1, 3 + 2, 2 + 3, and 1 + 4.

A. 4 + 1 and 1 + 4 configurations

In these configurations for the $[[5, 1, 3]]_5$ code, the fidelity of the state decoded by Bob is

$$F_{4+1} = p_1^4 p_2 + 4p_1^3 p_2 (1 - p_1) + p_1^4 (1 - p_2) + 6p_1^2 p_2 (1 - p_1)^2 f_1(p_d) + 4p_1^3 (1 - p_1)(1 - p_2) + (1 - P_{s_1})/5^5, \quad (4)$$

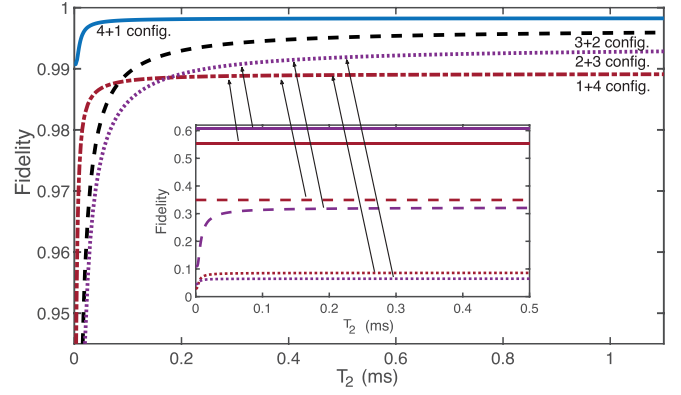


FIG. 3. Fidelity of the state decoded by Bob when Alice encodes her state using the $[[5, 1, 3]]_5$ QRS code in a quantum aggregation scenario for $L_1 = 1$ km and $L_2 = 3$ km versus the coherence time T_2 . The blue solid curve (red dash-dotted curve) refers to the 4 + 1 (1 + 4) configuration in which Alice distribute four (one) qudits into the shorter channels and one (four) qudits in the longer channels, respectively, whereas the dashed yellow curve (dotted purple curve) refers to the 3 + 2 configuration in which Alice distributes three (two) qudits into the shorter channels and three (two) qudits in the longer ones, respectively. In the inset, we plot the contributions to the fidelity of the probability of losing zero (solid curves), one (dashed curves), and two (dotted curves) qudits for the 1 + 4 and 2 + 3 configurations.

and

$$F_{1+4} = p_2^4 p_1 + 4p_2^3 p_1 (1 - p_2) + p_2^4 (1 - p_1) + 6p_2^2 p_1 (1 - p_2)^2 f_2(p_d) + 4p_2^3 (1 - p_2)(1 - p_1) + (1 - P_{s_2})/5^5, \quad (5)$$

where $P_{s_{1(2)}} = p_{1(2)}^4 p_{2(1)} + 4p_{1(2)}^3 p_{2(1)} (1 - p_{1(2)}) + p_{1(2)}^4 (1 - p_{2(1)}) + 6p_{1(2)}^2 p_{2(1)} (1 - p_{1(2)})^2 + 4p_{1(2)}^3 (1 - p_{1(2)})(1 - p_{2(1)})$ and $f_{1(2)}(p_d)$ being a contribution to the fidelity when two or one qudits are dephasing, respectively.

Comparing Eq. (4) with Eq. (5) one can see that the expressions of the two fidelities are almost identical except for the fourth term, which is multiplied by $f_{1,2}(p_d)$, respectively, whose analytical expression is given in Appendix B. What is important, however, is that $f_1(p_d) \leq f_2(p_d)$ and only equal at $p_d = 0, 1$. This is due to the fact that the term $f_1(p_d)$ can be considered as the fidelity of a density matrix in which two qudits are dephasing whereas $f_2(p_d)$ takes into account the dephasing of a single qudit. Hence in this later case, less information is lost. However, the dominant term in both Eqs. (4) and (5) is the no-loss term, hence, F_1 is higher than F_2 for any value of the dephasing time T_2 , as shown in Fig. 3. Therefore, it is more advantageous to distribute more qudits into the shorter path as well as what we obtained for the three-dimensional code.

B. 3 + 2 and 2 + 3 configurations

It is now interesting to analyze the 3 + 2 and 2 + 3 configurations of the $[[5, 1, 3]]_5$ QRS code. The respective fidelities

are

$$\begin{aligned}
 F_{3+2} = & p_1^3 p_2^2 + 3p_1^2 p_2^2 (1 - p_1) f_3(p_d) + 2p_1^3 p_2 (1 - p_2) \\
 & + 3p_1 p_2^2 (1 - p_1)^2 f_2(p_d) + p_1^3 (1 - p_2)^2 \\
 & + 6p_1^2 p_2 (1 - p_1) (1 - p_2) f_1(p_d) + (1 - P_{s_1})/5^5,
 \end{aligned} \quad (6)$$

and

$$\begin{aligned}
 F_{2+3} = & p_2^3 p_1^2 + 3p_2^2 p_1^2 (1 - p_2) f_3(p_d) + 2p_2^3 p_1 (1 - p_1) \\
 & + 3p_2 p_1^2 (1 - p_2)^2 f_1(p_d) + p_2^3 (1 - p_1)^2 \\
 & + 6p_2^2 p_1 (1 - p_2) (1 - p_1) f_2(p_d) + (1 - P_{s_2})/5^5,
 \end{aligned} \quad (7)$$

where $P_s = p_{1(2)}^3 p_{2(1)}^2 + 3p_{1(2)}^2 p_{2(1)}^2 (1 - p_{1(2)}) + 2p_{1(2)}^3 p_{2(1)} (1 - p_{2(1)}) + 3p_{1(2)} p_{2(1)}^2 (1 - p_{1(2)})^2 + p_{1(2)}^3 (1 - p_{2(1)})^2 + 6p_{1(2)}^2 p_{2(1)} (1 - p_{1(2)}) (1 - p_{2(1)})$.

Figure 3 shows that, even in this configuration, it is more convenient to use more qudits in the shorter path. In fact, F_1 (dashed yellow curve) is higher than F_2 (dotted purple curve) for any value of T_2 . Further, Fig. 3 shows that at $T_2 \geq 0.16$ ms the fidelity of the 2 + 3 configuration outperforms the fidelity of the 1 + 4 configuration. This can be explained with the fact that some terms of Eq. (7) are much more affected by the dephasing channel than Eq. (5). In fact, in the inset of Fig. 3 we plot for those two configurations, the contributions to the fidelity coming from the probability of losing zero (solid curves), one (dashed curves), and two (dotted curves) qudits. We expect that for large values of T_2 the probability of not losing any qudit is higher in the 2 + 3 configuration (purple solid curve of the inset) because less qudits are traveling in the longer channel compared to the 1 + 4 configuration (red solid curve of the inset) whereas the loss terms must be smaller. However, at lower values of T_2 , the contribution of losing one qudit for the 2 + 3 configuration is strongly affected by dephasing whereas the one of the 1 + 4 configuration does not depend on it. As regards the probability of losing two qudits, the dephasing channel affects both configurations with the 2 + 3 being slightly lower. The stronger impact of the decoherence on the 2 + 3 configuration also explains the behavior of the crossing points at which the fidelity of the 1 + 4 configuration is equal to the fidelity of the 2 + 3 configuration, as shown in Fig. 4. Here one can see that regardless the initial value of L_1 the crossing points occur at higher values of L_2 (which corresponds to lower p_2) when T_2 decreases.

Now assuming that a user can send one qudit per unit of time, this analysis shows that with a more even distribution of qudits (for instance, 3 + 2 or 2 + 3) one can obtain faster communication rates while reducing the quality of the transmitted state when compared to the 4 + 1 configuration while obtaining higher fidelity of the 1 + 4 configuration. However, at low values of T_2 the 1 + 4 configuration outperforms the 3 + 2 and the 2 + 3 configurations. When the fidelity is the main figure of merit is then fundamental in determining the value of the coherence time of the quantum memories at the receiver node to guarantee a certain threshold fidelity.

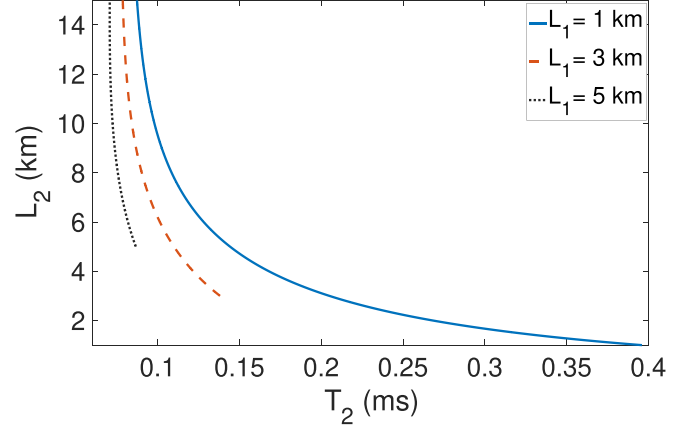


FIG. 4. Length of path 2 versus the decoherence time T_2 for the point at which the fidelity of the 1 + 4 configuration (red dash-dotted curve of Fig. 3) equals that of the 2 + 3 configuration (purple dotted curve of Fig. 3) for $L_1 = 1$ km (solid blue curve), $L_1 = 3$ km (dashed red curve), and $L_1 = 5$ km (dotted black curve). Note that the curves are shown for $L_2 > L_1$ according to the assumption that the length of path 2 is always bigger than that one of path 1.

C. $[[7, 1, 4]]_7$ QRS code

Let us now explore the performance of the large $[[7, 1, 4]]_7$ QRS code. Figure 5 shows the fidelities of all configurations of the $[[7, 1, 4]]_7$ QRS code, where the solid blue curve, the dashed yellow curve, and the green square dots refer to the case in which a higher number of qudits travel in the shorter channels whereas the dotted yellow curve, the blue

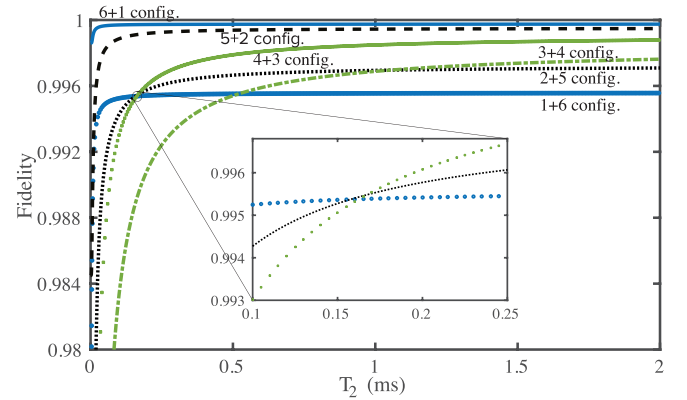


FIG. 5. Fidelity of the state received by Bob when Alice encodes her state using the $[[7, 1, 4]]_7$ QRS code in a quantum aggregation scenario for $L_1 = 1$ km and $L_2 = 3$ km. The blue solid curve (blue dots) refers to the 6 + 1 (1 + 6) configuration in which Alice distribute six (one) qudits into the shorter channels and one (six) qudits in the longer channels, respectively; the dashed yellow curve (dotted yellow curve) refers to the 5 + 2 configuration in which Alice distribute five (two) qudits into the shorter channels and two (five) qudits in the longer ones, respectively; the green square dots (dash-dotted green curve) refers to the 4 + 3 configuration in which Alice distribute four (three) qudits into the shorter channels and three (four) qudits in the longer ones, respectively. In the inset we plot the portion of the graph in which the 1 + 6, 2 + 5, and 4 + 3 configurations cross.

dots, and the green dash-dotted curve refer to the case in which the smaller number of qudits travel in longer channels. One can notice the following common features shared with the $[[5, 1, 3]]_5$ QRS case illustrated above. First, the case in which more qudits travel in the shorter path has higher fidelity than the other case for any value of T_2 . This is mainly due to the contribution of the no-loss term, which is the dominant term in the expressions of the fidelities. Then, when the qudits are almost equally distributed between the two channels (for instance, the $3 + 2$ configuration of the $[[5, 1, 3]]_5$ QRS code, or the $4 + 3$ configuration of the $[[7, 1, 4]]_7$ QRS code) the fidelities are much more affected by the dephasing. As a consequence, these fidelities will reach the asymptotic limit of $T_2 \rightarrow \infty$ at higher values of T_2 as shown in Fig. 5 (for instance, the purple dotted curve in Fig. 3 and the green dots and dash-dotted curve in Fig. 5).

Then, as well as the case of the $[[5, 1, 3]]_5$ QRS code, there is a crossing point in which the fidelities of different configurations intersect. The inset of Fig. 5 shows that this dephasing crossing point, T_2^c , occurs at $T_2^c = 0.16$ ms. This can be explained with a very similar motivation given in the $[[5, 1, 3]]_5$ QRS code case. In fact, the loss terms in the fidelity's expressions of the configurations in which the qudits are more evenly distributed depend on the dephasing channel much more than the loss terms of the uneven distributions. Hence, the corresponding fidelities assume high values at $T_2 \rightarrow \infty$ and very low values at $T_2 \rightarrow 0$ for the even distribution cases leading to a crossing point with the fidelity of the uneven case. This is an interesting feature of the aggregation network because one user can achieve a faster communication rate, sending more qudits simultaneously the more even is the distribution, while having better fidelities than the more uneven distribution case for certain values of T_2 . However, when the highest value of fidelity is required, then a more uneven distribution is preferred. This aspect can play an important role for some quantum communication systems in which a trade-off between the fidelity of the transmitted states and the transmission rate is the key factor, such as in several quantum key distribution schemes [6–9]. Therefore, for such systems optimizing the secret key rate could be a useful figure of merit to assess the performance of tomorrow's quantum network.

IV. CONCLUSION AND DISCUSSION

Distributing physical resources over multiple channels of different lengths in a quantum aggregation scenario will require the use of quantum memories to store the states arriving earlier. The decoherence process occurring in the memories will partially destroy the stored information before the delayed state arrives. Here we analyze the effect of such a delay time in a QRS code having dimensions of three, five, and seven, respectively. For these codes, we analytically calculate the fidelity of the final state as a function of the channel loss and the dephasing time for different configurations in which the resources are evenly or unevenly distributed over two paths of different length. We expect that for large values of the decoherence time T_2 the fidelities will reach an asymptotic optimal value regardless the length of the channels. In particular, we obtain that for $T_2 > 1$ ms the fidelities of all the configurations analyzed in this work asymptotically reach

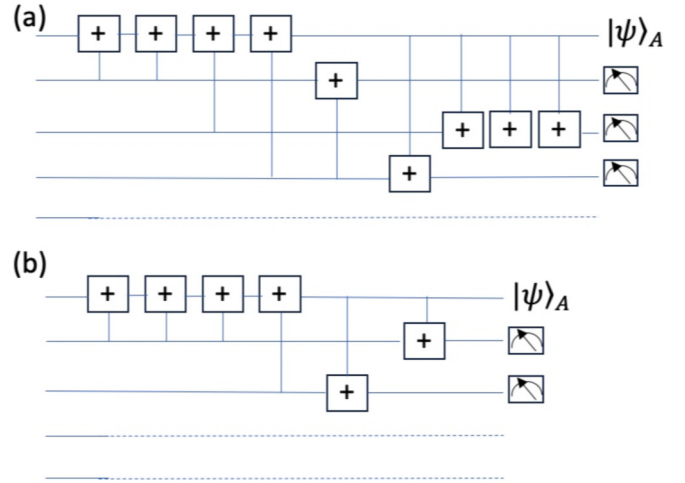


FIG. 6. Decoding circuit of the $[[5, 1, 3]]_5$ QRS code when (a) one qudit and (b) two qudits are lost, respectively. The dashed lines refer to the loss of a qudit. The symbol “+” refers to the sum mod 5 gate.

their optimal value. This threshold for the coherence time is vastly reachable with today's technology using, for instance, ion qubits [35], superconducting cavities [36], nuclear qubits of NV centers [37], and ensemble-based quantum memories [38]. We also analyze the behavior of such fidelities at a fixed value of the coherence time when the length difference between the two paths increases. In this case we obtain an asymptotic value for the fidelity when the majority of the qudits travels across the shorter path regardless of the value of the coherence time. However, when most of the qudits travel in the longer path we determine the largest achievable distance of such a path, which is strongly affected by the coherence time. We show that while quantum aggregation allows users in a quantum network to exchange information faster, the impact of a temporal delay in the received states can have a detrimental effect on the quality of the transmitted information. In addition, the configurations analyzed in this work can potentially provide a guideline on the architecture of quantum networks. Future works might consider using other error-correction codes with quantum aggregation due to its versatility as well as adding more paths connecting users.

ACKNOWLEDGMENT

This project was made possible through the support of the Moonshot R&D Program Grants No. JPMJMS2061 and No JPMJMS226C and JSPS KAKENHI Grant No. JP21H04880.

APPENDIX A: DECODING PROCEDURES

In this Appendix we illustrate the procedure to recover the state sent by Alice for the $[[5, 1, 3]]_5$ and $[[7, 1, 4]]_7$ QRS codes, respectively, in a lossy channel. Figure 6 shows the circuit that Bob applies to the encoded state sent by Alice when Fig. 6(a) illustrates the situation involving the loss of a single qudit and Fig. 6(b) the loss of two qudits. The gates represent a sum modulo 5 between two qudits of dimension five. After these gates are applied the remaining

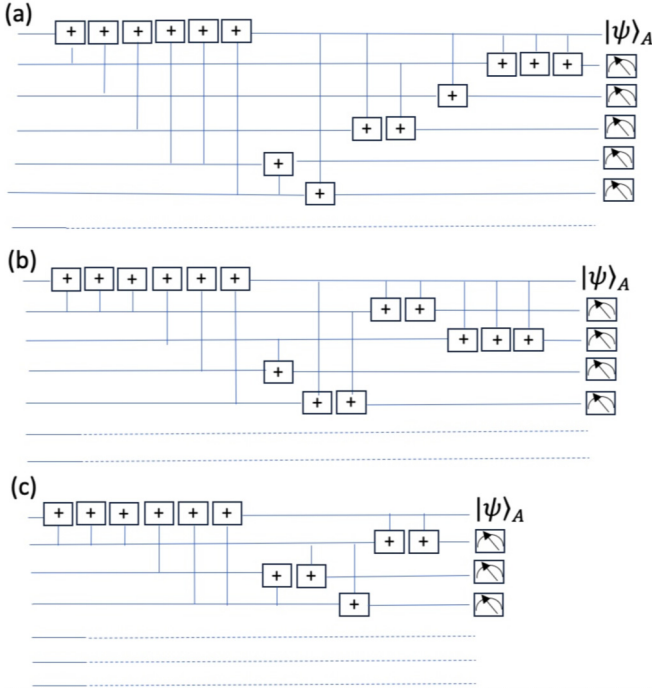


FIG. 7. Decoding circuit of the $[[7, 1, 4]]_7$ QRS code when (a) one qudit, (b) two qudits, and (c) three qudits are lost, respectively. The dashed lines refer to the loss of a qudit. The symbol “+” refers to the sum mod 7 gate.

qudits except the first one are measured in the computational basis. These measurements will ideally project the first qudit into the state $|\psi\rangle_A = \alpha_0|0\rangle + \alpha_1|1\rangle + \alpha_2|2\rangle + \alpha_3|3\rangle + \alpha_4|4\rangle$. Similarly, it is possible to retrieve the initial state of Alice for the $[[7, 1, 4]]_7$ QRS code with the decoding circuits shown in Figs. 7(a), 7(b), and 7(c), which correspond to the loss of one, two, and three qudits, respectively.

APPENDIX B: FIDELITIES AFTER DEPHASING

Here, we derive the general approach we use to calculate the fidelity of the $[[3, 1, 2]]_3$ QRS code when the density matrix of the state undergoes a dephasing channel. We then derive the terms that depend on the dephasing for the $[[5, 1, 3]]_5$ and $[[7, 1, 4]]_7$ QRS codes.

Alice initially encodes her physical state $|\psi\rangle_A = \alpha_0|0\rangle + \alpha_1|1\rangle + \alpha_2|2\rangle$ into the logical state $\rho_L = |\psi\rangle_L\langle\psi|_L$ and sends it to Bob over lossy channels, having transmission probabilities p_1 and p_2 , respectively. After the channel loss, the mixed density matrix can be expressed as a sum of density matrices multiplied by the loss probability, i.e.,

$$\rho_L \rightarrow \rho' = p_1^2 p_2 \rho_0 + p_1 p_2 (1 - p_1) \rho_1 + p_1 p_2 (1 - p_1) \rho_2 + p_1^2 (1 - p_2) \rho_3 + (1 - P_s) I_3, \quad (\text{B1})$$

where ρ_0 , ρ_1 , ρ_2 , and ρ_3 are the density matrices resulting from the loss of no qudit, the first qudit, the second, or the third qudit, respectively, while I_3 is the normalized identity operator of the Hilbert space spanned by the three qudits. We assume that the terms of the density matrix ρ' corresponding to the loss of two and three qudits are given by I_3 . The fidelity of the state given by Eq. (B1) is, therefore, a lower

bound of the total fidelity. Now, the density matrices ρ_1 and ρ_2 undergo a depolarization channel given by $\rho_{1,2} \rightarrow \rho'_{1,2} = (1 - p_d) \rho_{1,2} + p_d I_{1,2} \text{Tr}_{1,2}(\rho_{1,2})$, where $I_{1,2}$ is the identity of the Hilbert space spanned by qudits 1 and 2, respectively. Substituting $\rho'_{1,2}$ in Eq. (B1) we obtain

$$\rho' \rightarrow \rho(p_d) = p_1^2 p_2 \rho_0 + p_1 p_2 (1 - p_1) \rho'_1 + p_1 p_2 (1 - p_1) \rho'_2 + p_1^2 (1 - p_2) \rho_3 + (1 - P_s) I_3. \quad (\text{B2})$$

Bob applies the decoding procedure described in Muralidharam *et al.* [34], which ideally restores the initial state of Alice $|\psi\rangle_A$. The fidelity, F , is given by $F = {}_A \langle \psi | \rho(p_d) | \psi \rangle_A$.

We now show the derivation of the term $f_1(p_d)$ of Eq. (4). To this end, let us assume that the encoded state of the $[[5, 1, 3]]_5$ QRS code loses the first two qudits. The resulting state is then given by $\rho_l = \sum_{i=0}^5 |\psi\rangle_i \langle\psi|_i$, where

$$\begin{aligned} |\psi\rangle_0 &= \alpha_0|000\rangle + \alpha_1|341\rangle + \alpha_2|132\rangle + \alpha_3|423\rangle + \alpha_4|214\rangle, \\ |\psi\rangle_1 &= \alpha_0|111\rangle + \alpha_1|402\rangle + \alpha_2|243\rangle + \alpha_3|034\rangle + \alpha_4|320\rangle, \\ |\psi\rangle_2 &= \alpha_0|222\rangle + \alpha_1|013\rangle + \alpha_2|304\rangle + \alpha_3|140\rangle + \alpha_4|431\rangle, \\ |\psi\rangle_3 &= \alpha_0|333\rangle + \alpha_1|124\rangle + \alpha_2|410\rangle + \alpha_3|201\rangle + \alpha_4|042\rangle, \\ |\psi\rangle_4 &= \alpha_0|444\rangle + \alpha_1|230\rangle + \alpha_2|021\rangle + \alpha_3|312\rangle + \alpha_4|103\rangle. \end{aligned}$$

We now apply a depolarization channel to ρ_l and we obtain $\rho_l \rightarrow \rho'_l = (1 - p_d)^2 \rho_l + p_d (1 - p_d) I_{1(2)} \text{Tr}_1(\rho_l) + p_d (1 - p_d) I_{2(1)} \text{Tr}_2(\rho_l) + p_d^2 I_{12} \text{Tr}_{1,2}(\rho_l)$, where $I_{1(2)}$ is the identity operator of the Hilbert space spanned by the qudit 1(2) and $I_{12} = I_1 \otimes I_2$. Bob will apply the decoding procedure of Fig. 6 to the state ρ'_l obtaining a decoded state ρ''_l . The contribution of ρ''_l to the fidelity of Eq. (4), $f_1(p_d)$ will be:

$$\begin{aligned} f_1(p_d) &= {}_A \langle \psi | \rho''_l | \psi \rangle_A = \langle \psi | {}_A \rho(p_d) | \psi \rangle_A \\ &= \frac{1}{20 \left(\frac{5}{4} - 2p_d + p_d^2 \right)} \left[4 \left(4 \sum_{i=0}^4 \alpha_i^4 + 13 \sum_{i,j=0}^4 \alpha_i^2 \alpha_j^2 \right) p_d^2 \right. \\ &\quad \left. - 20 \left(2 \sum_{i=0}^4 \alpha_i^4 + 5 \sum_{i,j=0}^4 \alpha_i^2 \alpha_j^2 \right) p_d + 25 \right]. \quad (\text{B3}) \end{aligned}$$

It is straightforward to see that $f_1(p_d)$ has a minimum at $\alpha_0 = \alpha_1 = \alpha_2 = \alpha_3 = \alpha_4 = 1/\sqrt{5}$, which is the numerical value we have used to find the fidelities of Eqs. (4) and (5). The derivation of all the other terms due to dephasing follow a similar approach, hence, we only give here the final result:

$$\begin{aligned} f_2(p_d) &= \frac{1}{5 - 4p_d} \left[5 - 2 \left(2 \sum_{i=0}^4 \alpha_i^4 + 5 \sum_{i,j=0}^4 \alpha_i^2 \alpha_j^2 \right) p_d \right], \\ f_3(p_d) &= \frac{1}{(5 - 4p_d)^2} \left[2 \left(8 \sum_{i=0}^4 \alpha_i^4 + 25 \sum_{i,j=0}^4 \alpha_i^2 \alpha_j^2 \right) p_d^2 \right. \\ &\quad \left. - 20 \left(2 \sum_{i=0}^4 \alpha_i^4 + 5 \sum_{i,j=0}^4 \alpha_i^2 \alpha_j^2 \right) p_d + 25 \right]. \end{aligned}$$

The contributions to the fidelity that depend on p_d of the $[[7, 1, 4]]_7$ QRS code are:

$$g_1(p_d) = \frac{342(\frac{7}{6} - p_d)}{7(49 - 30p_d^3 + 108p_d^2 - 126p_d)} \left[\frac{2}{19} \left(6 \sum_{i=0}^4 \alpha_i^4 + 19 \sum_{i,j=0}^4 \alpha_i^2 \alpha_j^2 \right) p_d^2 - 42 \left(2 \sum_{i=0}^4 \alpha_i^4 + 5 \sum_{i,j=0}^4 \alpha_i^2 \alpha_j^2 p_d + \frac{49}{57} \right) \right],$$

$$g_2(p_d) = \frac{1}{6(\frac{7}{6} - p_d)} \left[7 - 2 \left(3 \sum_{i=0}^4 \alpha_i^4 + 7 \sum_{i,j=0}^4 \alpha_i^2 \alpha_j^2 \right) p_d \right],$$

$$g_3(p_d) = \frac{1}{(6p_d - 7)^3} \left[2 \left(108 \sum_{i=0}^4 \alpha_i^4 + 343 \sum_{i,j=0}^4 \alpha_i^2 \alpha_j^2 \right) p_d^3 - 42 \left(18 \sum_{i=0}^4 \alpha_i^4 + 49 \sum_{i,j=0}^4 \alpha_i^2 \alpha_j^2 \right) p_d^2 + 294 \left(3 \sum_{i=0}^4 \alpha_i^4 + 7 \sum_{i,j=0}^4 \alpha_i^2 \alpha_j^2 \right) p_d - 343 \right],$$

$$g_4(p_d) = \frac{1}{(49 - 35p_d + 49p_d^2)} \left[p_d^2 - 7 \left(5 \sum_{i=0}^4 \alpha_i^4 + 14 \sum_{i,j=0}^4 \alpha_i^2 \alpha_j^2 \right) p_d + 49 \right],$$

$$g_5(p_d) = \frac{1}{(6p_d - 7)^2} \left[3 \left(18 \sum_{i=0}^4 \alpha_i^4 + 49 \sum_{i,j=0}^4 \alpha_i^2 \alpha_j^2 \right) p_d^2 - 28 \left(3 \sum_{i=0}^4 \alpha_i^4 + 7 \sum_{i,j=0}^4 \alpha_i^2 \alpha_j^2 \right) p_d + 49 \right].$$

-
- [1] L. Childress and R. Hanson, *MRS Bull.* **38**, 134 (2013).
[2] M. S. Blok, N. Kalb, A. Reiserer, T. H. Taminiau, and R. Hanson, *Faraday Discuss.* **184**, 173 (2015).
[3] H. J. Kimble, *Nature (London)* **453**, 1023 (2008).
[4] C. H. Bennett and G. Brassard, *Theor. Comput. Sci.* **560**, 7 (2014).
[5] N. Sangouard, C. Simon, H. de Riedmatten, and N. Gisin, *Rev. Mod. Phys.* **83**, 33 (2011).
[6] A. K. Ekert, *Phys. Rev. Lett.* **67**, 661 (1991).
[7] J. Qiu, *Nature (London)* **508**, 441 (2014).
[8] H. Lo, *Science* **283**, 2050 (1999).
[9] W.-Y. Hwang, *Phys. Rev. Lett.* **91**, 057901 (2003).
[10] W. J. Munro, K. Azuma, K. Tamaki, and K. Nemoto, *IEEE J. Sel. Top. Quantum Electron.* **21**, 6400813 (2015).
[11] M. Nielsen and I. Chuang, *Quantum Computation and Quantum Information* (Cambridge University Press, Cambridge, England, 2000).
[12] C. Bennett and D. DiVincenzo, *Nature (London)* **404**, 247 (2000).
[13] S. J. Devitt, A. M. Stephens, W. J. Munro, and K. Nemoto, *Nat. Commun.* **4**, 2524 (2013).
[14] R. Raussendorf and H. J. Briegel, *Phys. Rev. Lett.* **86**, 5188 (2001).
[15] E. Knill, *Nature (London)* **434**, 39 (2005).
[16] L.-M. Duan and R. Raussendorf, *Phys. Rev. Lett.* **95**, 080503 (2005).
[17] C. L. Degen, F. Reinhard, and P. Cappellaro, *Rev. Mod. Phys.* **89**, 035002 (2017).
[18] L. A. Lugiato, A. Gatti, and E. Brambilla, *J. Opt. B* **4**, S176 (2002).
[19] D. S. Simon, G. Jaeger, and A. V. Sergienko, *Int. J. Quantum Inf.* **12**, 1430004 (2014).
[20] T. C. Ralph, A. J. F. Hayes, and A. Gilchrist, *Phys. Rev. Lett.* **95**, 100501 (2005).
[21] A. G. Fowler, D. S. Wang, C. D. Hill, T. D. Ladd, R. Van Meter, and L. C. L. Hollenberg, *Phys. Rev. Lett.* **104**, 180503 (2010).
[22] D. Gottesman, A. Kitaev, and J. Preskill, *Phys. Rev. A* **64**, 012310 (2001).
[23] W. J. Munro, A. M. Stephens, S. J. Devitt, K. A. Harrison, and K. Nemoto, *Nat. Photon.* **6**, 777 (2012).
[24] K. Azuma, K. Tamaki, and H. K. Lo, *Nat. Commun.* **6**, 6787 (2015).
[25] S. Muralidharan, J. Kim, N. Lutkenhaus, M. D. Lukin, and L. Jiang, *Phys. Rev. Lett.* **112**, 250501 (2014).
[26] L. Jiang, J. M. Taylor, K. Nemoto, W. J. Munro, R. Van Meter, and M. D. Lukin, *Phys. Rev. A* **79**, 032325 (2009).
[27] M. Fanizza, F. Kianvash, and V. Giovannetti, *Phys. Rev. Lett.* **125**, 020503 (2020).
[28] M. Rosati, A. Mari, and V. Giovannetti, *Nat. Commun.* **9**, 4339 (2018).
[29] M. E. Shirokov, *J. Math. Phys.* **58**, 102202 (2017).
[30] N. Lo Piparo, M. Hanks, K. Nemoto, and W. J. Munro, *Phys. Rev. A* **102**, 052613 (2020).
[31] M. Grassl, W. Geiselmann, and T. Beth, *International Symposium on Applied Algebra, Algebraic Algorithms, and Error-Correcting Codes* (Springer, New York, 1999), p. 231.
[32] N. Lo Piparo, W. J. Munro, and K. Nemoto, *Phys. Rev. A* **99**, 022337 (2019).
[33] One can always increase the length of the shorter path at Bob by adding a local delay. This, however, is not a realistic

solution as one would need to dynamically adjust both paths and they could still fluctuate in length over time. This becomes even less practical when multiple paths are connecting the nodes.

- [34] S. Muralidharan, C.-L. Zoo, L. Li, J. Wen, and L. Jiang, *New J. Phys.* **19**, 013026 (2017).
- [35] P. Wang, C.-Y. Luan, M. Qiao, M. Um, J. Zhang, Y. Wang, X. Yuan, M. Gu, J. Zhang, and K. Kim, *Nat. Commun.* **12**, 233 (2021).
- [36] O. Milul, B. Guttel, U. Goldblatt, S. Hazanov, L. M. Joshi, D. Chausovsky, N. Kahn, E. Çiftyürek, F. Lafont, and S. Rosenblum, *PRX Quantum* **4**, 030336 (2023).
- [37] K. Nemoto, M. Trupke, S. J. Devitt, B. Sharfenberger, K. Buczak, J. Schmiedmayer, and W. J. Munro, *Sci. Rep.* **6**, 26284 (2016).
- [38] L. Chen, Z. Xu, W. Zeng, Y. Wen, S. Li, and H. Wang, *Sci. Rep.* **6**, 33959 (2016).